Spectroelectrochemical Characterization of Cytidine Nucleolipid Biomimetic Membranes Supported on Gold (111) Electrodes

Julia Alvarez-Malmagro[a,b], ZhangFei Su[b], J. Jay Leitch[b], Francisco Prieto[a], Manuela Rueda[a], Jacek Lipkowski[b]

[a] Department of Physical Chemistry, University of Seville, C/Professor García González nº 2, 41012 Seville, Spain.

[b] Department of Chemistry, University of Guelph, Guelph, Ontario, Canada N1G 2W1.

Corresponding authors:

Francisco Prieto: dapena@us.es

Manuela Rueda: marueda@us.es

Jacek Lipkowski:jlipkows@uoguelph.ca

Abstract

The effect of the electrode potential on the orientation and conformation of 1,2-dipalmitoyl-*sn*-glycero-3-cytidine monolayer deposited onto gold (111) electrode surface was described. The potential of zero free charge (E_{pzc}) for the monolayer covered electrode was determined to be -0.2 V vs SCE. The differential capacitance and charge density data indicated that the monolayer is stable at the electrode surface when (E-E_{pzc}) > 0.0 V. At negative rational potentials, a progressive detachment (electrodewetting) of the monolayer occurs. The monolayer is fully detached from the electrode surface at (E-E_{pzc}) < -0.6 V. The conformation and orientation of the acyl chains and orientation of the cytosine moiety were determined with the help of photon polarization modulation infrared reflection absorption spectroscopy (PM-IRRAS). The IR measurements demonstrate that the acyl chains are predominantly in the gel phase in the adsorbed state and tilted at an angle of ~30º with respect to the electrode surface normal. The tilt angle of the acyl chains increases when the film is detached from the gold surface indicating that the monolayer becomes more disordered. At (E-E_{pzc}) > 0.0 V, the plane of the cytosine moiety assumes a small angle of ~20º with respect to the surface normal. At negative potentials, the tilt angle of the cytosine fragment increases and rotates. With the help of DFT calculations, these changes were explained by the repulsion of the positive pole of the cytosine permanent dipole moment by the positively charged gold surface and its attraction to the metal surface at negative electrode potentials. This work provides unique information for the future development of sensors based on the molecular recognition of nucleoside targets.

1. Introduction

This study is part of our efforts to understand adsorption and molecular recognition between complementary nucleoside bases at the gold electrode surface.[1–6] The goal of these studies was to understand the influence of the static electric field on molecular recognition reactions. The major problem is that nucleic acids adsorb to the bare gold electrode surface and it is difficult to differentiate between the gold-base and base-base interactions. This work describes the electrochemical and PM-IRRAS studies of 1,2-dipalmitoyl-*sn*-glycero-3-cytidine nucleolipid (Figure 1) monolayers deposited onto gold electrode surfaces using the Langmuir-Schaefer technique. In this architecture, the cytidine moiety of the nucleolipid is oriented towards the solution and separated from the gold surface by acyl chains of the lipid. Consequently, this design provides a means to investigate the influence of the static electric field on the orientation and monitor the reactivity of the base moiety by eliminating the interactions of the target nucleic acids with the metal.

Nucleolipid monolayers spread at the air-solution interface have been successfully used to study the interactions between complementary nucleobases.[7–10] Several papers have described the application of nucleolipid monolayers to study the molecular recognition between cytosine and guanine.[7–9] These IRRAS and SERS studies have provided direct spectroscopic evidence regarding the nature of interactions between complementary nucleic acid base pairs.

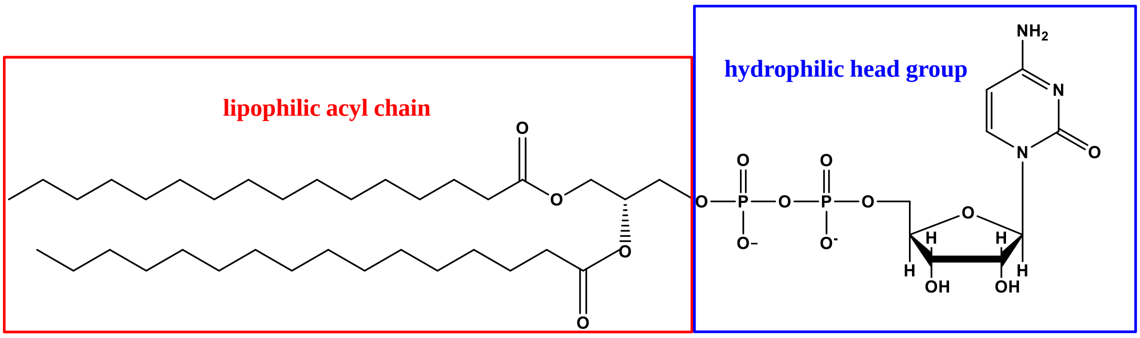

Figure 1. Structure of 1, 2-dipalmitoyl-*sn*-glycero-3-cytidine diphosphate nucleolipid (16:0 CDP DG)

The objective of this work was to employ electrochemistry and PM-IRRAS to characterize the physical structure and behavior of 1,2-dipalmitoyl-*sn*-glycero-3-cytidine diphosphate nucleolipid monolayers deposited on the surface of gold (111) electrodes using the Langmuir-Schaefer (LS) technique. The electrochemical measurements monitor the stability and kinetics of the LS films and the PM-IRRAS spectra provide information about the orientation of the acyl chains and cytidine moiety of the nucleolipid with respect to the electrode surface. Additionally, the IR spectra also give insight into the conformation of the acyl chains. The data acquired in this work provides a basis for subsequent studies focused on understanding the mechanism of guanine attachment to oriented cytidine lipid monolayers. Although

spectroscopic techniques were used to study nucleolipid monolayers at the air-solution interface in the past, the investigations in this work were performed at the metal-solution interface, which is more relevant in terms of the future development of nucleic acid-based biosensors. Furthermore, the quantitative measurements described in this work can also provide unique insights into the dependency of host-guest molecular recognition reactions on the orientation of the polar head group of the host.

2. Experimental.

2.1. Reagents, solutions, electrodes and materials.

1, 2-dipalmitoyl-*sn*-glycero-3-cytidine diphosphate (16:0 CDP DG), obtained from Avanti Polar Lipids, was dissolved in chloroform to give a final stock concentration of 1 mg mL^{-1}. Sodium fluoride powder (BioXtra, 99%) was purchased from Sigma-Aldrich and cleaned in an UV ozone chamber (Jelight UVO cleaner) for 15 minutes to oxidize and remove any organic impurities prior to electrolyte preparation. Cytosine (Sigma Aldrich), cytidine 5'-diphosphate sodium salt (Sigma Aldrich) were used without additional purification. For the electrochemical measurements, all aqueous electrolyte solutions were prepared from ultrapure water (resistivity > 18.2 MΩ cm) purified by a Milli-Q UV plus (EMD Millipore) water system. D_2O (Cambridge Isotope Laboratories) was used to prepare the electrolyte solutions for the PM-IRRAS and transmission IR experiments.

Home-grown gold (111) single crystals were used as the working electrodes and Ag/AgCl electrodes (saturated KCl, Pine Research Instrumentation) were used as the reference electrodes in both the electrochemical and PM-IRRAS experiments. Prior to each experiment, the single crystal face of the gold (111) electrode was flame-annealed in a propane torch and cooled in air under the plume of the flame. A flame-annealed gold coiled wire was used as the counter electrode in the electrochemical experiments while a Pt foil was implemented as the counter electrode in the PM-IRRAS experiments. All spectroelectrochemical experiments were performed at room temperature (20 ± 2 °C) and the applied potentials have been converted to the saturated calomel electrode (SCE) scale by correcting the measured potential with the potential difference between the SCE and Ag/AgCl potentials (-0.045 V).

All glassware, including the electrochemical cell, was either soaked in a potassium permanganate bath overnight or cleaned in a mixed concentrated hot acid bath (3-parts H_2SO_4 to 1-part HNO_3 v/v) for 2 h. The glassware was then thoroughly rinsed with Milli-Q water. The Teflon components of the spectroelectrochemical cell were cleaned in piranha solution (3-parts H_2SO_4 to 1-part H_2O_2 v/v) and meticulously rinsed with Milli-Q water.

2.2. LB trough: pressure-area isotherms and sample preparation.

Surface pressure-area isotherms were recorded at the air-solution interface using a Langmuir trough (KSV NIMA Technology Ltd) controlled by KSV LB5000 software. The trough was equipped with two symmetric barriers and a Wilhelmy plate (surface area is 243 cm^2) constructed from a fresh piece filter paper. The experiments were performed at 24 ± 1 and 44 ± 1 °C on a pure water subphase.

Prior to the electrochemical and PM-IRRAS measurements, Langmuir-Schaefer (LS) deposition was employed to transfer the monolayer onto the gold (111) surface. The water subphase was then heated to 44 ± 1 °C. The 1,2-dipalmitoyl-*sn*-glycero-3-cytidine diphosphate chloroform solution was spread onto the air-water interface using a Hamilton microsyringe and the solvent was allowed to evaporate for a minimum of 15 min. At this temperature the monolayer was in the liquid expanded state allowing for a good transfer onto the gold electrode. The monolayer was compressed to a surface pressure of 30 mN m^{-1} and transferred to the (111)-face of the gold electrode by the horizontal touch technique (LS method). The electrode was dried for 1 h before further experimentation. The monolayer transferred at the gold (111) surface should have the same packing density as the monolayer formed at the air-solution interface.[11] The LS method ensures that the nucleolipid molecules were oriented with the cytidine group oriented towards the solution.

2.3. Electrochemical instrumentation and measurements.

Electrochemical measurements were performed using a HEKA PG 590 potentiostat /galvanostat and a lock-in amplifier (EG & G Instruments 7265 DSP). All data was collected using a plug-in acquisition card NI PCI-6052E and custom written software. The electrochemical measurements were carried out in an all-glass three-electrode cell using the hanging meniscus configuration. The cell was purged with argon for 30 min before applying a potential to the working electrode. The purity of electrolyte was verified by recording differential capacitance curves (DC) of the electrolyte solution and comparing with those previously reported in the literature.[12,13] The DC curves were measured using a scan rate of 5 mV s^{-1} superimposed on an ac perturbation with a frequency of 25 Hz and rms amplitude of 5 mV. The capacitance was calculated from the in-phase and out-of-phase components of the ac signal treating the electrochemical interface as a capacitor and resistor in series (RC circuit).

The surface charge densities at the gold (111) electrode were measured using chronocoulometry.[13,14] Preliminary experiments determined that the potential of zero charge (E_{pzc}) for the monolayer covered electrode was equal to -0.20 V vs SCE. The charge densities for the monolayer covered electrode were performed using the following series of potential

steps: 1) the base (E_b) potential was held at E=-0.20 V vs SCE for a period of 60 s and then stepped to final potential (E_f) for a period of 200 ms. The charge difference between E_b and E_f was measured by integration of the charging current curves. The potential was then returned to E_b for another waiting time of 60 s and was stepped again to E_f which vale was changing from -0.15 V to 0.4 V vs SCE in 50 mV increments. 2) Similar train of potential steps was applied from E_b=-0.20 V vs SCE to E_f which value was changing from -0.25 V to -0.4 V vs SCE. 3) Finally a train of potential pulses was applied from E_b variable from -0.4 V to -0.85 V vs SCE to a constant final potential -0.9 V vs SCE at which a total desorption of the monolayer took place. This program of potential pulses ensured a minimum perturbation of the monolayer structured by reducing to minimum potential steps to desorption of the monolayer. For the supporting electrolyte, the charge density curve was determined by stepping from a variable E_b to a constant E_f=-0.9 V vs. SCE, waiting 60 s at E_b between each consecutive potential step. The potential steps were applied in 0.05 V intervals.

2.4. Spectra collection and processing.

2.4.1. Transmission spectra and sample preparation.

The transmission spectra were acquired using a home-made cell with a circular CaF_2 windows separated by 10 μm Teflon spacer. In all cases, a total of 1000 scans were collected using a resolution of 4 cm^{-1}. The Barenholz method was used to prepare vesicles solution for transmission experiments.[15] 1,2-dipalmitoyl-*sn*-glycero-3-cytidine diphosphate solution (10 mg ml^{-1}) in chloroform was added to a test tube, which was vortexed and dried under a stream of argon for 2 h. This procedure created a thin film of nucleolipid coating on the inside wall of the test tube. Finally, 2 ml of D_2O was added into the test tube and the mixture was sonicated at 40 ± 1 °C for a duration of 40 minutes to form 5mg mL^{-1} solution of unilamellar 1,2-dipalmitoyl-*sn*-glycero-3-cytidine diphosphate vesicles.

2.4.2. PM-IRRAS spectra.

PM-IRRAS measurements were performed using a Nicolet Nexus 870 (ThermoFisher) spectrometer equipped with an external tabletop optical mount, MCT-A detector, photoelastic modulator (Hinds Instruments PM-90 with a II/ZS50 ZnSe 50 kHz optical head) and a sampling demodulator (GWC Instruments Synchronous Sampling Demodulator). The tabletop optical module (TOM) box was purged with a dry, CO_2-free air, provided by a purge gas generator (Parker Balston), for ~5 h prior to and throughout the duration of the experiment. The spectra were collected at a temperature of 20 ± 2 °C using in-house software, an Omnic macro, and a digital-to-analog converter (Omega) to control the potentiostat (EG&G PAR362). The IR window was a 1 in. CaF_2 equilateral prism (Janos Technology), which was first cleaned with

water and methanol before being placed in the UV-ozone cleaner for 10 min prior to the experiments.

The electrode was transferred to the cell filled with 0.1 M NaF in D_2O. To remove O_2, the solution was de-aerated with argon for 20 min. The electrode was then pressed against the IR window to create the thin film configuration. The applied potential was varied from 0.16 V vs. SCE to -0.75 V vs. SCE with steps of 0.1 V. At each potential, a total of 4000 scans were collected using a resolution of 4 cm^{-1}. The PM-IRRAS measurements were performed with a photoelastic modulator (PEM) set to half-wave retardation at 1600 cm^{-1} for the head group spectral region and 2900 cm^{-1} for the CH stretching region. The angle of incidence of the infrared beam were set 60° for the head group region and 56° for the CH stretching region, to obtain a large enhancement of the mean square electric field strength (MSEFS) of p-polarized radiation on the electrode surface. The electrolyte thickness was ~ 4 μm as determined from the procedure discussed previously in literature.[16]

The intensity of the PM-IRRAS spectrum, ΔS, is proportional to the absorbance, A, of molecules adsorbed on the electrode surface and defined as:

$$\Delta S = \frac{2(I_s - I_p)}{I_s + I_p} = 2.3\varepsilon\Gamma_\varepsilon \quad (1)$$

where I_s and I_p are the intensities of the s- and p-polarized radiation, Γ_ε is the surface concentration of the adsorbed species and ε is the decadic molar absorption coefficient of the adsorbed species. The details of the PM-IRRAS measurement and the data processing were described previously.[16]

2.4.3. Simulation of the PM-IRRAS spectra of the monolayer.

The PM-IRRAS spectra of the 1,2-dipalmitoyl-*sn*-glycero-3-cytidine diphosphate monolayers were simulated using a model of four homogeneous parallel phases (gold/nucleolipid film/D_2O/CaF_2) using software that solves the Fresnel equation using the transfer matrix method.[17] The optical constants of gold, D_2O and CaF_2 were taken from the literature.[18,19] The optical constants of the 1,2-dipalmitoyl-*sn*-glycero-3-cytidine diphosphate were obtained from the transmission spectra. The thickness of the 1,2-dipalmitoyl-*sn*-glycero-3-cy11tidine were assumed to be 3 nm, which is equal to a half of the thickness of DPPC bilayer.[20]

The directions of the transition dipoles for vibrations of the cytosine moiety of the nucleolipid were determined from DFT calculations of vibrational spectra for cytidine. The hybrid functional PBE [21] and the basis set 6-311++G(d,p) as present in the Gaussian 09 package

has been used in these calculations.[22] The effect of the solvent on the isolated molecule was treated by the continuum polarization model (PCM).

3. Results and discussion.

3.1. Compression isotherm studies.

The properties of 1,2-dipalmitoyl-*sn*-glycero-3-cytidine nucleolipid monolayers at the air-water interface were studied by recording surface pressure-molecular area isotherms. Figure 2 shows the compression isotherms for the nucleolipid on the air-water interface at 24 ± 1 and 44 ± 1 °C. The inset to Figure 2 shows the compression modulus calculated from the compression isotherms and defined as:[23]

$$C_s^{-1} = -A\frac{d\pi}{dA} \quad (2)$$

where A is the area per molecule and π is the surface pressure of the monolayer. A phase transition seen as a minimum on the compression modulus plots takes place at surface pressure of ~20 mN m^{-1} and 30 mN m^{-1} for the isotherms recorded at 24 °C and 44 °C. At surface pressures lower than the minimum point, the C_s^{-1} values are less than 60 mN m^{-1} indicating that the monolayer exists in the liquid-expanded (LE) state. The C_s^{-1} values increase to over 200 mN m^{-1} at pressures higher than the minimum point, signifying that a densely packed gel state is formed.[24] The film collapses at ~ 72 mN m^{-1} for 24 °C and at ~ 68 mN m^{-1} for 44 °C. The high values of the collapse pressure suggest strong interaction between polar heads that stabilize the monolayer. The collapse of monolayers is observed at mean cross sectional area ~60 $Å^2$. The geometric cross sectional area of the two acyl chains corresponds to ~40 $Å^2$.[25] Larger value of the experimental cross section area indicates that acyl chains in the monolayer are tilted. The tilt is caused by a larger cross section area of the head than the cross section area of the tails.[25] For the electrochemical and spectroelectrochemical studies, the monolayer was transferred from the air-solution to the gold surface at a film pressure of 30 mN m^{-1} (corresponding to liquid crystalline state). At this surface pressure, the mean molecular area corresponds to 72 $Å^2$.

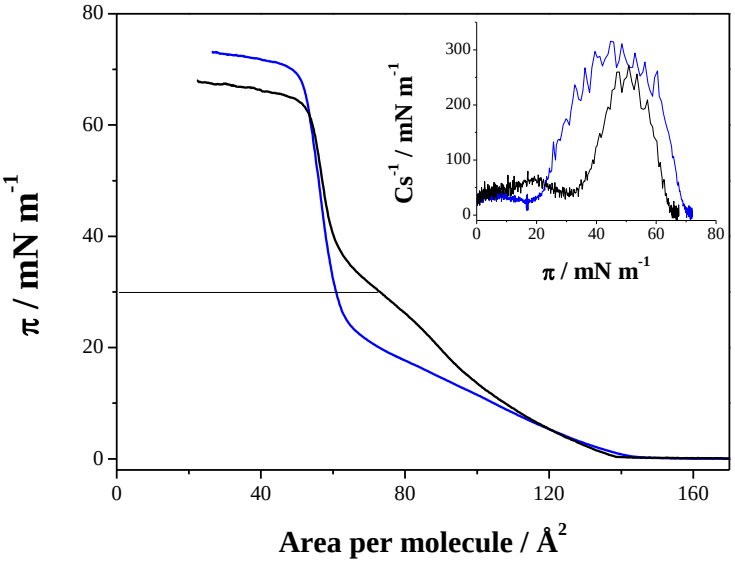

Figure 2. Compression isotherms plotted vs the mean molecular area for 1, 2-dipalmitoyl-*sn*-glycero-3-cytidine nucleolipid monolayers at 24 °C (blue line) and at 44 °C (black line). A constant pressure of 30 mN m^{-1} was selected as the transfer pressure to ensure a packed 1,2-dipalmitoyl-*sn*-glycero-3-cytidine monolayer was deposited onto the gold (111) electrode surface. The inset shows the calculated compression modulus for the two monolayers as a function of the surface pressure.

3.2. Electrochemical measurements.

Differential capacitance and charge density curves (determined from chronocoulometric experiments) were used to characterize the behavior of the 1,2-dipalmitoyl-*sn*-glycero-3-cytidine diphosphate monolayer as a function of the electrode potential. The differential capacitance curves are plotted in Figure 3a) and the charge density curves are presented in Figure 3b). The differential capacitance plot shows that the monolayer is adsorbed to the gold (111) electrode surface at potentials between 0.4 V and -0.4 V vs. SCE. At potentials more negative than -0.4 V vs. SCE, the differential capacitance curve corresponding to the monolayer-covered electrode begins to merge with the curve for the monolayer-free electrode indicating that the monolayer is desorbed from the electrode surface. Electro-dewetting of the film is completed at ~ -0.7 V vs. SCE. At a potential of -0.8 V vs. SCE, the monolayer is detached from the gold surface. At this potential, the capacitance of the electrode initially covered by the monolayer becomes equal to the capacitance measured in the absence of the film. This behavior was previously observed for films of lipids using chronocoulometry,[26] elastic light scattering,[27] and neutron reflectivity measurements.[28] Differential capacitance of the electrode surface with a monolayer of the nucleolipid is a function of the electrode potential E and the surface concentration of the nucleolipid Γ as described by the equation:

$$C = \frac{d\sigma}{dE} = \left(\frac{\partial\sigma}{\partial E}\right)_{\Gamma} + \left(\frac{\partial\sigma}{\partial \Gamma}\right)_{E}\frac{d\Gamma}{dE} = \left(\frac{\partial\sigma}{\partial E}\right)_{\Gamma} + \left(\frac{\partial\sigma}{\partial \Gamma}\right)_{E}\frac{d\Gamma}{dt}\frac{dt}{dE} \quad (3)$$

The term $\left(\frac{\partial\sigma}{\partial E}\right)_{\Gamma}$, capacitance at a constant coverage is referred to as the true capacitance and the term $\left(\frac{\partial\sigma}{\partial \Gamma}\right)_{E}\frac{d\Gamma}{dE}$ is referred to as a pseudo capacitance which magnitude depends on the change of the surface concentration with potential. The magnitude of the pseudo capacity depends on the rate of adsorption desorption or the rate of a change in the surface state represented in the last term of equation 3 by $\frac{d\Gamma}{dt}$. If the kinetics are slow the pseudo capacity term is reduced in magnitude or disappears. The differential capacitance curve in Figure 3a do not display characteristic adsorption/desorption or surface reorganization peaks. This behavior indicates that the kinetics of these processes are slow and the capacitance curve recorded at a single frequency 25 Hz is dominated by the true capacitance $\left(\frac{\partial\sigma}{\partial E}\right)_{\Gamma}$.

Figure 3b) shows the charge densities for the electrode without and with the nucleolipid monolayer. The charge density curve of the monolayer-covered electrode intersects with the zero line at -0.20 V vs. SCE. This number corresponds to the potential of zero charge (E_{pzc}). The E_{pzc} of the gold electrode in the absence of the film is equal to +0.20 V vs. SCE. The E_{pzc} electrode covered by the nucleolipid film is significantly shifted in the negative direction. This shift is expected since the nucleolipid carries a negative charge. Adsorption of anions shifts the pzc in the negative direction and hence the behavior displayed by the nucleolipid is characteristic of an anion adsorption.[29] The capacitance curve displays a minimum around the E_{pzc}. The minimum value corresponds to 11.6 μF cm^{-2}. This value is typical for a film of anionic lipids.[30] In contrast to differential capacitance measurements in which a small 5 mV rms perturbation was employed, large potential steps were used in charge density measurements. Therefore large driving forces for adsorption/desorption and surface reorientation were applied accelerating these processes.

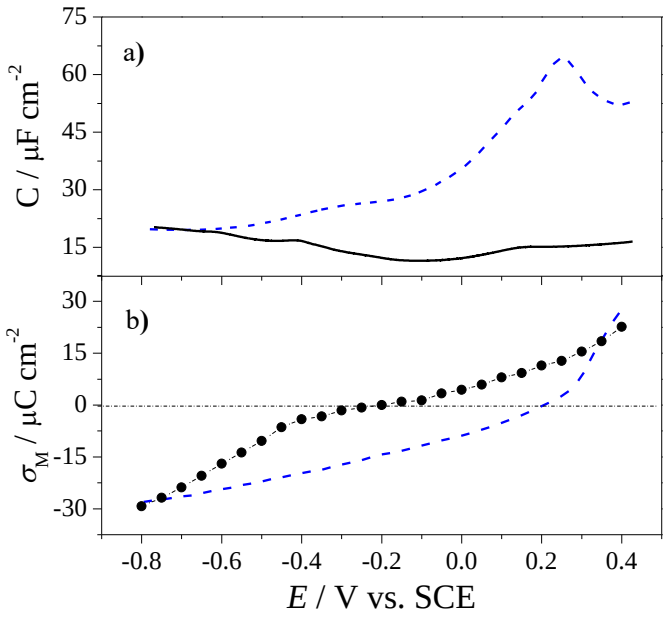

Figure 3. a) Differential capacity and b) charge density curves for a bare gold (111) (blue dashed line) and a 1,2-dipalmitoyl-*sn*-glycero-3-cytidine monolayer covered gold (111) electrode (solid line and black points) in a 0.1 M NaF/H_2O electrolyte.

3.3. PM-IRRAS results

PM-IRRAS technique provides information about the conformation and orientation of nucleolipid molecules allowing for structural interpretation of the electrochemical data. It is convenient to discuss the spectral regions with bands of the acyl chains of the lipid and bands of the polar head separately.

3.3.1 Acyl chain region between 3000-2800 cm^{-1}.

The spectral region between 3000 and 2800 cm^{-1} contains CH stretching bands of the acyl chains. These vibrations provide information regarding conformation of the chains and their tilt angle with respect to the surface normal. Since the spectra of the acyl chains region are similar to the spectra that were published in the literature[16] they are presented in Figure S1 of the Supporting Information. The spectra consist of four bands centered at 2851 ± 1 cm^{-1} ($\nu_s(CH_2)$), 2874 ± 1 cm^{-1} ($\nu_s(CH_3)$), 2924 ± 1 cm^{-1} ($\nu_{as}(CH_2)$) and 2959 ± 1 cm^{-1} ($\nu_{as}(CH_3)$) contribute to this broad spectral envelope.[16] The two shoulders on higher and lower frequency sides of the methylene asymmetric band correspond to the Fermi resonances (FR). Figures 4b) shows a sample deconvolution of the CH spectral region. The peak positions and widths of the bands are listed in Table SI 1 of the Supporting information. These values are potential-independent. For DPPC, a phospholipid with the same acyl chain length, in a gel state, the positions of the $\nu_s(CH_2)$ and $\nu_{as}(CH_2)$ band centers are equal to 2850 and 2920 cm^{-1},

respectively.[31] These numbers are close to band frequencies in the spectra of the monolayer of 1,2-dipalmitoyl-*sn*-glycero-3-cytidine diphosphate suggesting that the nucleolipid is predominantly in the gel state. In addition, the full width at half maximum (FWHM) is equal to 13 ± 3 cm^{-1} for $\nu_s(CH_2)$ and to 19 ± 2 cm^{-1} for $\nu_{as}(CH_2)$, which is consistent with gel phase monolayers where the acyl chains primarily adopt an all-*trans* conformation.[32,33]

The integrated intensities of symmetric and asymmetric vibrations for methylene groups can be used to calculate the average angle between the *trans* fragments of the chains in the 1, 2-dipalmitoyl-*sn*-glycero-3-cytidine monolayer and the surface normal.[16] The average angles of the *trans* fragment of the acyl chains are plotted in Figure 4. When the monolayer is in the adsorbed state at potentials more positive than -0.3 V vs. SCE, the tilt angle has a value of ~30°, which is characteristic of well-ordered monolayer.[16] When the voltage applied to the electrode is in the range of -0.4 to -0.8 V vs. SCE, the tilt angle of the *trans* fragment increases to ~ 35°. The increase in the tilt angle at negative potentials indicates that desorption introduces disorder into the monolayer.

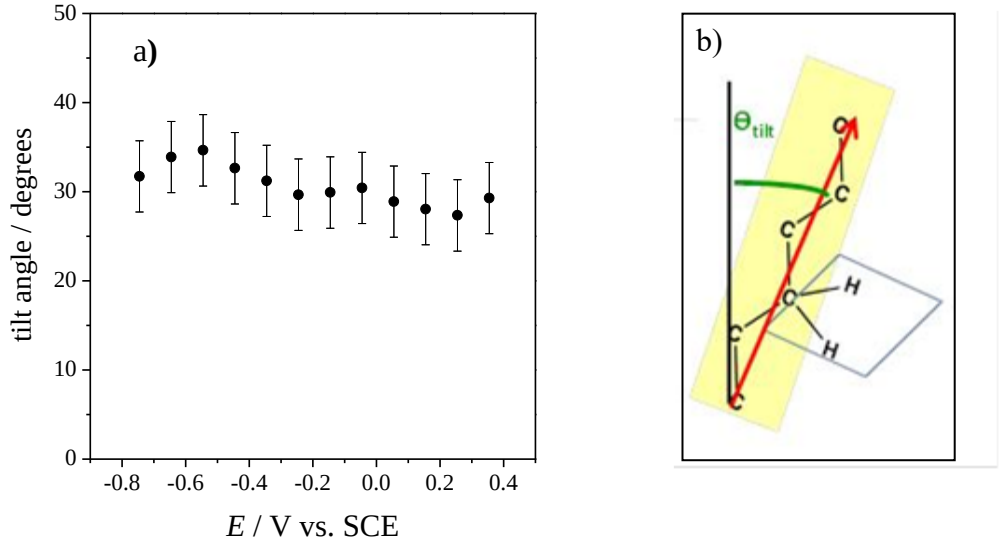

Figure 4. a) Tilt angle of the 1,2-dipalmitoyl-*sn*-glycero-3-cytidine nucleolipid monolayer at gold (111) plotted as a function of the electrode potential. b) Pictorial definition of the tilt angle for the backbone of the acyl chains.

3.3.2 Polar head region 1800-1400 cm^{-1}.

The 1800-1400 cm^{-1} region contains bands associated with the vibration modes of the polar head group. These bands contain information regarding the orientation and conformation of the polar head in the monolayer. Figure 5a) shows the PM-IRRAS spectrum of the polar head region of 1, 2-dipalmitoyl-*sn*-glycero-3-cytidine diphosphate monolayer on the gold (111) surface recorded at 0.16 V vs. SCE. For comparison purposes, Figure 5b) plots the spectrum of

a solution of vesicles of 1, 2-dipalmitoyl-*sn*-glycero-3-cytidine diphosphate in D_2O recorded in transmission mode. The two spectra are similar indicating that no major changes in the head group of the nucleolipid occur after transfer of the monolayer onto the gold electrode surface. To identify bands corresponding to the cytosine moiety of the polar head group, Figure 5c) plots the transmission spectrum of a 10 mM solution of cytosine and Figure 5d) plots transmission spectrum of cytidine 5'-diphosphate in a D_2O electrolyte. Both of these transmission spectra are in a good agreement with measurements previously published in the literature.[34–36]

The ~1650 cm^{-1} band of the cytidine spectrum (Figure 5d) is broader than the band at 1643 cm^{-1} in the spectrum of cytosine (Figure 5c). Furthermore, the band at ~1654 cm^{-1} in the spectrum of 16:0 CDP DG vesicles (Figure 5b) is even broader than in the spectrum of cytidine (Figure 5d). The broadening of this peak suggests that the band is complex. To resolve this issue, Figure 6 displays the Fourier self-deconvolution (FSD) of the 1750-1550 cm^{-1} spectral region. The FSD methodology reveals the sub-band structure by narrowing the bands.[37]

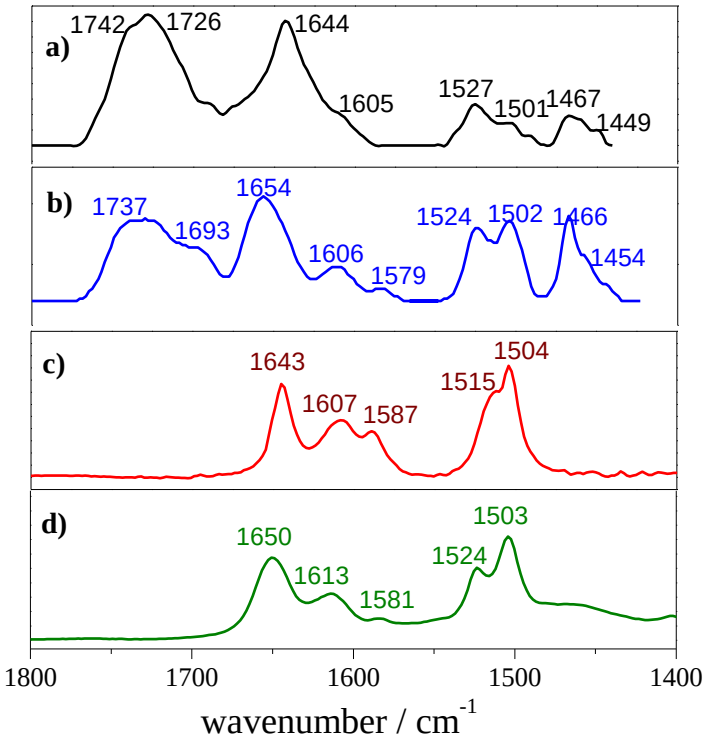

Figure 5. a) PM-IRRAS spectra of 1,2-dipalmitoyl-*sn*-glycero-3-cytidine diphosphate monolayer recorded at E = 0.16 V vs. SCE, b) transmission IR spectrum of 1,2-dipalmitoyl-*sn*-glycero-3-cytidine diphosphate vesicles in D_2O, c) transmission IR spectrum of a 10 mM solution of cytosine and d) spectrum of 5 mM solution of cytidine 5'-diphosphate in a 0.1 M NaF/D_2O electrolyte solution.

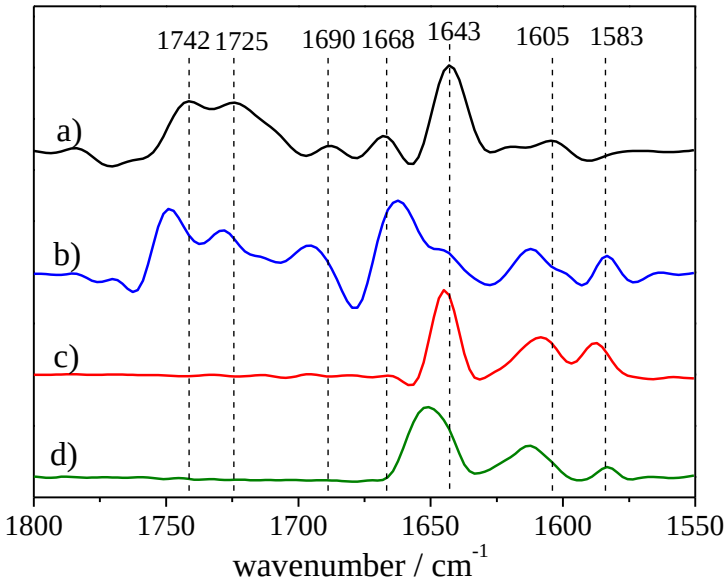

Figure 6. Fourier self-deconvolution (FSD) of: a) PM-IRRAS spectra of 1,2-dipalmitoyl-*sn*-glycero-3-cytidine monolayer at E = 0.16 V vs SCE; b) transmission IR spectrum of vesicles of 1,2-dipalmitoyl-*sn*-glycero-3-cytidine; c) transmission IR spectrum of cytosine and d) transmission spectrum cytidine 5-diphosphate.

In the 1650 cm^{-1} region, the PM IRRAS spectrum (Figure 6a) and the spectrum of vesicles (Figure 6b) have two bands at ~1668 and 1643 cm^{-1}. In contrast, the FSD spectrum for cytosine (Figure 6c) is narrow indicating the presence of only one band. However, the FSD spectrum of cytidine-5'-DP (Figure 6d) is significantly broader suggesting that it is more complex. The assignment of the cytosine spectral bands is well documented.[34,35,38–40] In the spectrum of vesicles and the PM IRRAS spectrum of the monolayer, the modes at ~1668 and 1643 cm^{-1} appear split. The splitting is more pronounced in the monolayer spectrum where the 16:0 CDP DG molecules are more tightly packed and better organized. Apparently, this splitting results from the lateral interactions between neighboring molecules. Additionally, two bands at 1648 and 1660 cm^{-1} were also observed in the IR spectrum of solid cytidine.[41] Alternatively, the splitting may be caused by the presence of two tautomers of cytosine moiety. Section SI 6 of the Supporting Information presents DFT calculations of spectra corresponding to two major tautomer of cytosine; keto-imino tautomer and keto-amino tautomer.[42]. The calculated spectra show that the presence of two tautomers may cause broadening or splitting of the ~1650 cm^{-1} band. They demonstrated that the IR band at ~1585 cm^{-1} of the experimental spectra can only be assigned to the keto-imino tautomer. However in the transmission spectrum of cytidine-5'-DP this band is weak and in the PM IRRAS spectra it is essentially absent, indicating that the PM IRRAS spectra are dominated by the keto-amino tautomer.

The assignments of the bands corresponding to the cytosine moiety in the spectra of Figure 5 are presented in Table 1. Not included in Table 1 are; the band at ~1467 cm^{-1} which corresponds to $\delta(CH_2)$ of the chains and bands at 1742 and 1726 cm^{-1} which correspond to the

non-hydrogen bonded and hydrogen bonded carbonyl group vibrations of the glycerol moiety.[43] The assignment of band at 1690 cm^{-1} is difficult, however, it is present in the spectrum of a solid cytidine-5'monophosphate[41], it was also observed in IR spectrum of matrix isolated cytosine[44] and in a DFT calculated spectrum.[45] A plausible assignment of this band could be to non-hydrogen bonded C=O group vibration. This would imply that a small fraction of C=O groups are not solvated by D_2O.

To study the influence of the electrode potential on the orientation of the cytosine moiety, the PM-IRRAS spectra of the 1, 2-dipalmitoyl-sn-glycero-3-cytidine monolayer were measured in the range of potentials between -0.75 V and 0.06 V vs. SCE.

Table. 1. Assignments of bands corresponding to cytosine moiety in the 1800-1400 cm^{-1} spectral region

Cytosine[34,35,38–44]		Cytidine-5DP[36,38,46,47]	16:0 CDP DG vesicles	16:0 CDP DG PM-IRRAS
Experimental	DFT calculations [42,]	Experimental	Experimental	Experimental
1643(νC=O)	1677 (keto amino), 1658 (keto-imino)	1650 (νC=O)	1665 (νC=O) 1644 (νC=O)	1668 (νC=O) 1644 (νC=O)
1607 (νC_5=C_6)	1602 (keto-amino), 1609 (keto-imino)	1613 (νC_5=C_6)	1606 (νC_5=C_6)	1611 (νC_5=C_6)
1587 (νC_4=N_7, νC_5=C_6)	1553 (keto-imino)	1581(νC_4=N_7) (keto-imino)	1579(νC_4=N_7) (keto-imino)	
1515 νC_4=C_5)	1489 (keto-amino)	1524 (νC_4=C_5)	1524 (νC_4=C_5)	1525 (νC_4=C_5)
1504 (νC_4-N_7)	1447 (keto- amino)	1502 (νC_4-N_7)	1502 (νC_4-N_7)	1503 (νC_4-N_7)

Position of the bands are given in cm^{-1}., 16:0 CDP DG -1,2-dipalmitoyl-*sn*-glycero-3-cytidine diphosphate

Figure 7a) shows the PM IRRAS spectra recorded at selected electrode potentials. The top spectrum in Figure 7a) is the spectrum of randomly oriented molecules calculated from optical constants for 3 nm thick nucleolipid film. Figure 7b) shows the deconvolution of the average PM-IRRAS spectrum using a mixture of Lorentzian-Gaussian functions. The deconvolution was assisted by calculating the second derivative and Fourier self-deconvolution of the PM-IRRAS spectrum presented in Figure S2 and 2D-COS presented in Figure S3 of the Supporting Information. These procedures provided information about the number of bands and their positions. The inset to Figure 7b) shows the band at ~1585 cm^{-1}. The intensity of this band is more than an order of magnitude lower than the intensity of the other bands in the spectrum.

This behavior confirms that the bands chiefly correspond to the keto-amino tautomer of the cytosine moiety. With the help of the spectra in Figures 6 and 7, five major bands at 1668, 1644; 1611, 1525 and 1503 cm^{-1} were identified.

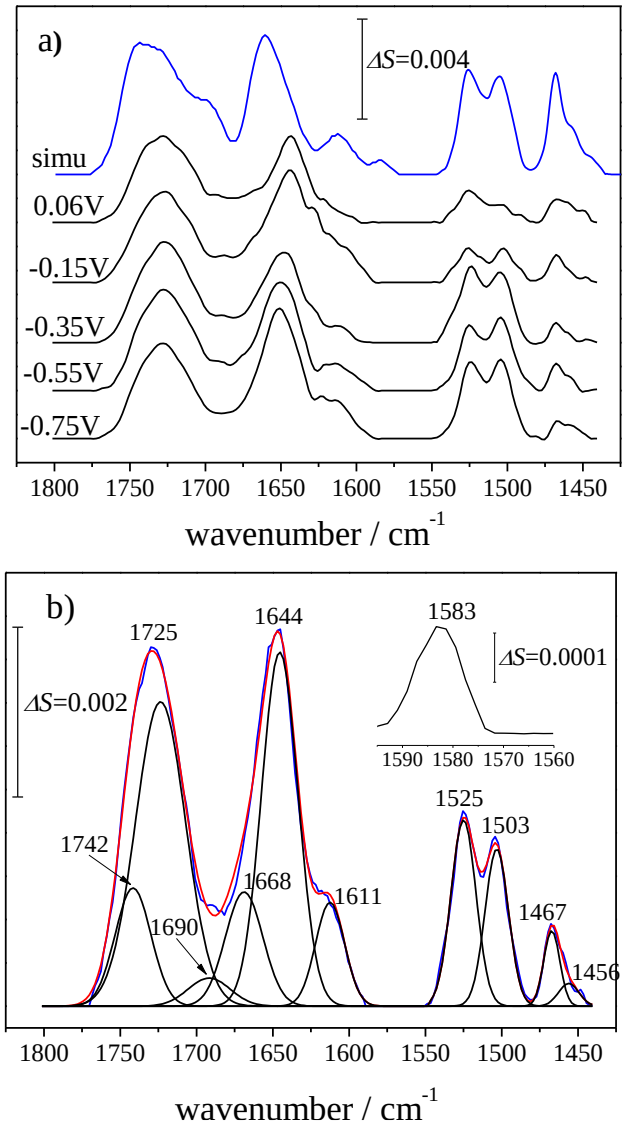

Figure 7. a) PM-IRRAS spectra of the 1,2-dipalmitoyl-*sn*-glycero-3-cytidine diphosphate nucleolipid monolayer at gold (111) surface in the 1800-1400 cm^{-1} region in 0.1 M NaF electrolyte at selected potentials. The top spectrum represents a randomly oriented 1,2-dipalmitoyl-*sn*-glycero-3-cytidine diphosphate monolayer providing a direct comparison with the experimental spectra. An offset was applied to the curves to avoid curves overlap. b) Deconvolution of the average PM-IRRAS spectrum of the monolayer of 1,2-dipalmitoyl-*sn*-glycero-3-cytidine diphosphate. The insert displays a zoomed fragment of the spectrum at 1585 cm^{-1} showing the appearance of a very weak spectral band.

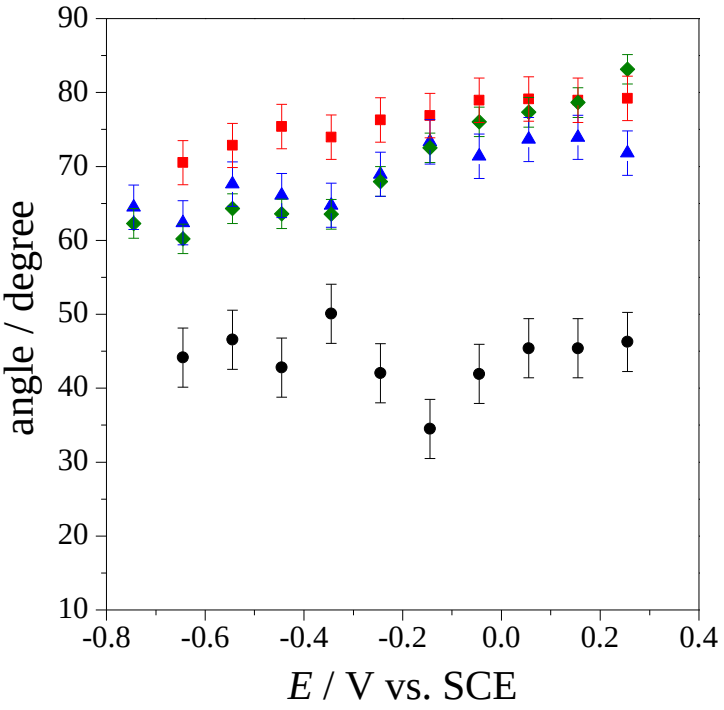

Figure 8. Angles between directions of transition dipoles and the surface normal corresponding to: 1668 (red squares), 1644 (black circles), 1525 (blue triangles) and 1503 cm^{-1} (green diamonds) band of the 1,2-dipalmitoyl-*sn*-glycero-3-cytidine diphosphate monolayer at the gold (111) electrode plotted as a function of the electrode potential.

The integrated intensity of bands in the 1800-1400 cm^{-1} region were used to determine the angle between the transition dipole of the IR band and the surface normal θ according to Equation 3

$$\frac{\int A_{\mathrm{exp}} d\bar{\nu}}{\int A_{\mathrm{calc}} d\bar{\nu}} = \frac{\cos^2 \theta}{\cos^2 55^{\circ}} \qquad (3)$$

In equation 3, $\int A_{\mathrm{exp}} d\bar{\nu}$ is the integrated intensity of the band in the PM-IRRAS spectrum and $\int A_{\mathrm{calc}} d\bar{\nu}$ is the integrated intensity of the same band calculated for randomly oriented molecules from optical constants of a solution of vesicles.[16,17] The angle between direction of the transition dipole of the scissoring band of the methyl groups in the acyl chain at 1466 cm^{-1} and surface normal (Figure S4 of the Supporting Information) shows a good agreement between angles of the $\delta(CH_2)$ and $\nu(CH_2)_s$. The transition dipoles of these two bands have the same direction and hence this agreement is an indication that the reported values are free of major errors of the data processing procedures.

Figure 8 plots the angles of transition dipoles for the 1668, 1644, 1525 and 1503 cm^{-1} bands of the cytosine moiety. The angles of bands at 1668, 1525 and 1503 cm^{-1} have similar large values indicating that the cytosine moiety is nearly parallel with respect to the monolayer surface. In contrast, the angles of the band at 1644 cm^{-1} have much smaller values, indicating

that transition dipole of this band is not located in the plane of the cytosine moiety. This behavior is consistent with the assignment of this band to the coupled vibrations of cytosine and D-ribose rings.[41] The bands at ~1525 and 1503 cm^{-1} are well resolved and their assignment to cytosine ring vibration is straightforward. Figure SI 5 of the Supporting Information shows that the ~1525 and 1503 cm^{-1} bands correspond to the keto-amino tautomeric form. In contrast, the bands at 1668 and 1644 cm^{-1} may have contributions from other tautomeric forms and are more sensitive to environmental changes. Therefore, the angles of the transition dipoles of 1525 and 1503 cm^{-1} bands were used for quantitative analysis of the potential dependent changes in the orientation of the cytosine moiety.

3.3.3 Orientation of the cytosine moiety

A recent study showed that two angles between the directions of a transition dipole and the surface normal corresponding to vibrations in the molecular plane (θ) can be used to determine the tilt angle of the molecular plane relative to the surface normal (α) and the angle between the transition dipole and the projection of the surface normal on the molecular plane (φ).[5] The angle φ provides information about rotation of the molecular plane of the molecule. The definition of angles, θ, α and φ is schematically described in Figure 9. The angles, θ, α and φ are related by the following expression:

$$\cos(\theta) = \cos(\alpha) \times \cos(\varphi) \quad (4)$$

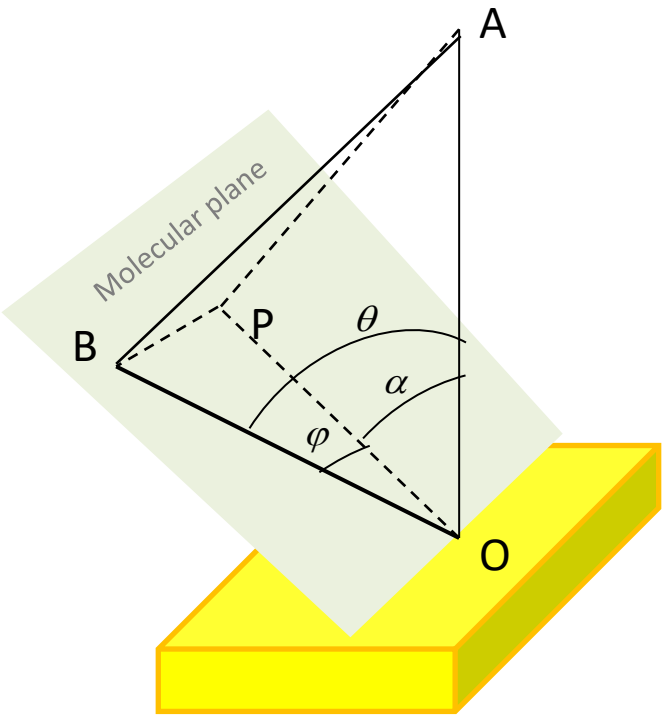

Figure 9. Schematic representation of the molecular plane and the directions normal to the electrode surface ($\overline{OA}$), projected normal to the molecular plane ($\overline{OP}$), projected normal to the surface onto the molecular plane ($\overline{AP}$) , direction of the transition dipole moment ($\overline{OB}$) and direction in the molecular plane parallel to the electrode surface. ($\overline{BP}$).

The DFT calculation provides the difference between the angles φ of two in plane vibrations ($|\varphi_1-\varphi_2|$). If angles θ_1 and θ_2 for these vibrations are known, the tilt angle of the molecular plane relative to the surface normal (α) and the angles φ_1 and φ_2 can be determined.[5]

With the help of DFT calculation, the difference $|\varphi_{1525}-\varphi_{1502}|$ was determined to be 68°. With this information, the tilt angle of the cytosine moiety α and the directions of the transition dipoles of the 1525 cm^{-1} and 1502 cm^{-1} bands relative to the surface normal projection onto the moiety plane were calculated and plotted in Figure 10.

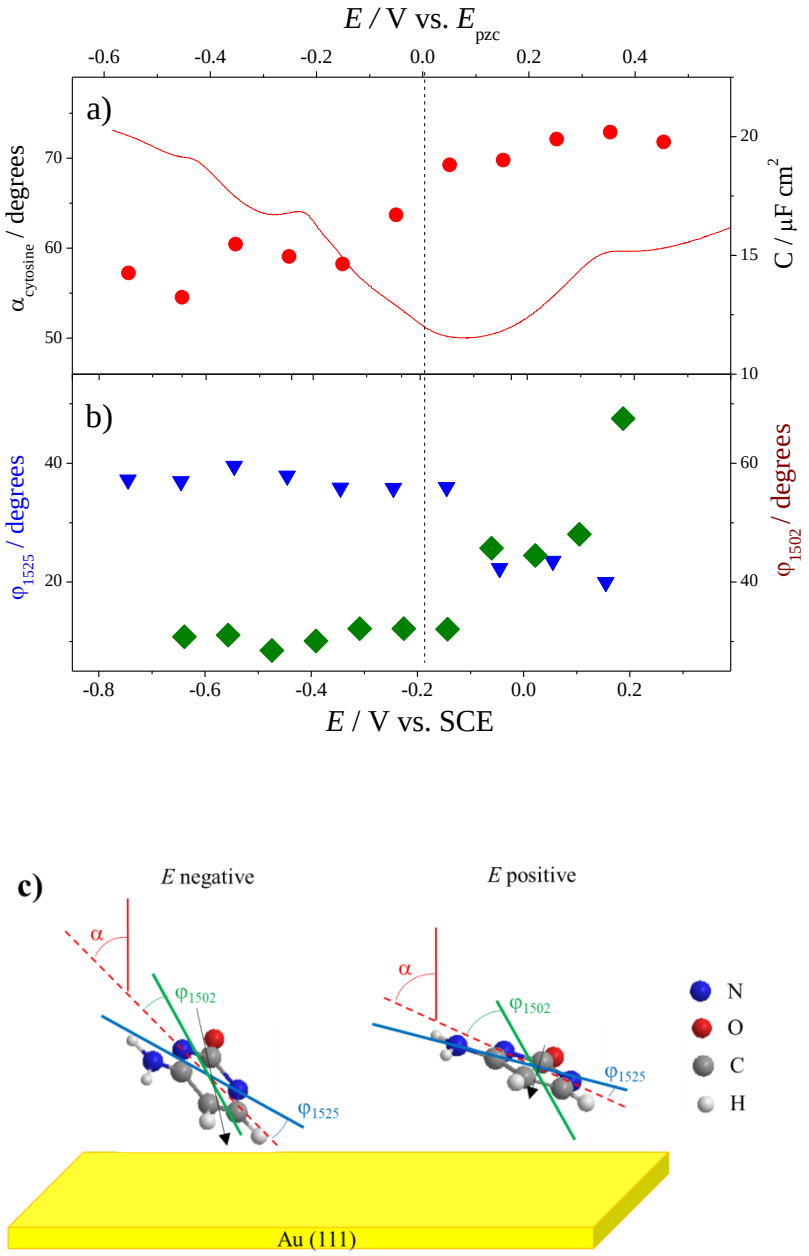

Figure 10. Potential dependence of angles corresponding to the cytosine fragment of the nucleolipid monolayer: a) Tilt angle of the molecular plane (solid circles) and differential capacitance curve taken from Figure 3. b) Angles between the projection of surface normal on the molecular plane and the transition dipole directions of the vibrations at 1502 cm^{-1} (dark green diamonds) and 1525 cm^{-1} (blue triangles). c) Qualitative picture of the cytosine moiety orientation at negative and positive rational potentials. The lines represent the directions of the electrode surface normal (solid red line), the projected surface normal on the molecular plane (dashed red line), the transition dipole of the vibration at 1502 cm^{-1} (green solid line) and the transition dipole of the vibration at 1525 cm^{-1} (blue solid line). The black arrow represents the permanent dipole of the cytosine moiety.

The angle between the plane of cytosine moiety and the surface normal is close to 70° at potentials more positive than -0.2 V vs. SCE and drops down to 60 - 55° at potentials more

negative -0.3 V vs. SCE. The change amounts to about 15 degrees and takes place in a narrow potential range between -0.2 V and -0.3 V vs. SCE. In Figure 10, the upper horizontal axis plots rational potential (E-E_{pzc}). Its values show that the change in the tilt of the cytosine moiety takes place at the potential of zero charge. At positively charged surface the plane of the cytosine moiety is nearly parallel to the surface while the angle is ~55^o at negative potentials. The angle 55^o may correspond to a random orientation. However, the tilt angles for the chains in Figure 4 show that the sample is oriented. Therefore, we interpret this angle as corresponding to the oriented sample. For the benefit of discussion, the solid line in Figure 10 a) plots the differential capacitance of the gold electrode covered by the nucleolipid monolayer previously displayed in Figure 3a). Figure 10a) shows that changes in the tilt of the cytosine moiety correlate well with changes of the differential capacitance. The tilt of ~70^o is observed at potentials where monolayer is adsorbed at the gold electrode surface and decreases at potentials where the monolayer becomes detached from the gold surface. These changes are also consistent with a change of the tilt of *trans* fragments of the acyl chains observed in Figure 4. The tilt of the chains increases at negative potentials indicating that they become less ordered in the desorbed state.

Figure 10b) shows changes in the rotation of cytosine plane with the electrode potential. The plane rotates approximately 10^o - 15^o within a very narrow range of potentials form -0.15 V to 0.05 V vs. SCE. At positive potentials, the direction of the transition dipole of the 1525 cm $^{-1}$ is nearly parallel to the projection of surface normal surface normal on the cytosine plane. At negative potentials, the rotation angle increases as the changes in the angle of direction of the transition dipole of the 1502 cm^{-1} band are decreasing. Schematic diagrams of these angles are provided in Figure 10c) to provide a visual interpretation of these changes. The direction of the permanent dipole of the cytosine moiety is marked in the diagrams as an arrow. The diagrams show that the decrease of α and rotation of the cytosine plane brings the positive pole of the permanent dipole closer to the electrode surface at negative potential and away from the surface at positive potential. In conclusion, the observed change of the tilt and rotation of the cytosine moiety induced by the applied potential can be explained by electrostatic interactions between the permanent dipole moment of cytosine and the electric field at the surface.

4. Summary and Conclusions.

A monolayer of 1,2-dipalmitoyl-*sn*-glycero-3-cytidine diphosphate was deposited at the gold (111) electrode surface. The differential capacitance and chronocoulometric measurements determined that the monolayer is stable at positive rational potentials and is progressively detached (electrodewetting) at negative rational potentials. PM-IRRAS experiments were performed to determine the conformation and orientation of acyl chains and the orientation of

the cytosine moiety as a function of the applied potential. The acyl chains assume a predominantly *trans* conformation and are tilted at ~30 ± 2° with respect to the surface normal in the adsorbed state. The tilt angle of the acyl chains increases by about 5° upon detachment at negative potentials. The changes in the orientation of the cytosine moiety are more pronounced. The plane of the molecule has a small ~20° angle with respect to the surface in the adsorbed state. This angle increases by ~15° during detachment of the monolayer at negative potentials. The change in the tilt is accompanied by rotation of the plane of cytosine moiety. With the help of DFT calculations, these changes are explained by electrostatic interactions between the positive pole of the permanent dipole of the cytosine moiety and the field at the electrode surface. At positive potentials, the orientation of the cytosine moiety ensures that the positive dipole points away from the surface and is directed towards the metal surface at negative potentials. The present results have strong relevance for investigations of molecular recognition in a sensor built by depositing monolayer of 1,2-dipalmitoyl-*sn*-glycero-3-cytidine diphosphate at the gold (111) electrode surface, which will be described in the future studies.

Acknowledgements

Financial supports from the Spanish Ministry of Economy and Competitiveness (CTQ2014-57515-C2-1-R) and from the Andalusian government (PAI-FQM202) are acknowledged. JAM acknowledges a FPU grant and a Visiting Academic grant from the Spanish Ministry of Science and Technology. JL acknowledges support of the Discovery grant from Natural Sciences and Engineering Council of Canada RG-03958.

Supporting Information

Figure SI 1 PM-IRRAS spectra in the CH stretching region of 1,2-dipalmitoyl-sn-glycero-3-cytidine and their deconvolution; Table S1 Positions and FWHMs for CH stretching bands in the monolayer of 1,2-dipalmitoyl-*sn*-glycero-3-cytidine; Figure S2 Second derivative and Fourier self deconvolution of the PM IRRAS spectrum of the monolayer of 1,2-dipalmitoyl-sn-glycero-3-cytidine assisting bands deconvolution; Figure S3 2DCOS of PM IRRAS spectra of the monolayer of 1,2-dipalmitoyl-*sn*-glycero-3-cytidine; Figure S4 Plot of angles between directions of transition dipoles and surface normal for CH_2 bands in the monolayer of 1,2-dipalmitoyl-*sn*-glycero-3-cytidine; Figure S5 Simulated IR spectra of deuterated cytosine tautomers.

5. Literature

(1) Prieto, F.; Alvarez-Malmagro, J.; Rueda, M.; Orts, J. M. Tautomerism of Adsorbed Thymine on Golg Electrodes: An in Situ Surface-Enhanced Infrared Spectroscopy Study. *Electrochim. Acta* **2016**, *201*, 300–310.

(2) Rueda, M.; Prieto, F.; Álvarez-Malmagro, J.; Rodes, A. Evidences of Adenine – Thymine Interactions at Gold Electrodes Interfaces as Provided by In-Situ Infrared Spectroscopy. *Electrochem. Commun.* **2013**, *35*, 53–56.

(3) Alvarez-Malmagro, J.; Prieto, F.; Rueda, M.; Rodes, A. In Situ Fourier Transform Infrared Reflection Absortion Spectroscopy Study of Adenine Adsorption on Gold Electrodes in Basic Media. *Electrochim. Acta* **2014**, *140*, 476–481.

(4) Alvarez-Malmagro, J.; Rueda, M.; Prieto, F. In Situ Surface-Enhanced Infrared Spectroscopy Study of Adenine-Thymine Co-Adsorption on Gold Electrodes as a Function of the PH. *J. Electroanal. Chem.* **2018**, *819*, 417–427.

(5) Prieto, F.; Su, Z.; Leitch, J. J.; Rueda, M.; Lipkowski, J. Quantitative Subtractively Normalized Interfacial Fourier Transform Infrared Reflection Spectroscopy Study of the Adsorption of Adenine on Au(111) Electrodes. *Langmuir* **2016**, *32* (16), 3827–3835.

(6) Prieto, F.; Alvarez-Malmagro, J.; Rueda, M. Electrochemical Impedance Spectroscopy Study of the Adsorption of Adenine on Au(111) Electrodes as a Function of the PH. *J. Electroanal. Chem.* **2017**, *793*, 209–217.

(7) Miao, W.; Luo, X.; Liang, Y. Molecular Recognition of 7-(2-Octadecyloxycarbonylethyl)-Guanine to Cytidine at the Air/Water Interface and LB Film Studied by Fourier Transform Infrared Spectroscopy. *Spectrochim. Acta Part A Mol. Biomol. Spectrosc.* **2003**, *59*, 1045–1050.

(8) Miao, W.; Luo, X.; Wu, S.; Liang, Y. Fourier Transform Infrared Spectroscopy Study on Order-Disorder Transition in Langmuir-Blodgett Films of 7-(2-Octadecyloxycarbonylethyl)Guanine before and after Recognition to Cytidine. *Spectrochim. Acta - Part A Mol. Biomol. Spectrosc.* **2004**, *60*, 413–416.

(9) Wang, Y.; Du, X.; Miao, W.; Liang, Y. Molecular Recognition of Cytosine- and Guanine-Functionalized Nucleolipids in the Mixed Monolayers at the Air-Water Interface and Langmuir-Blodgett Films. *J. Phys. Chem. B* **2006**, *110* (10), 4914–4923.

(10) Čoga, L.; Spindler, L.; Masiero, S.; Drevenšek-Olenik, I. Molecular Recognition of a Lipophilic Guanosine Derivative in Langmuir Films at the Air-Water Interface. *Biochim. Biophys. Acta - Gen. Subj.* **2017**, *1861*, 1463–1470.

(11) Garcia-Araez, N.; Brosseau, C. L.; Rodriguez, P.; Lipkowski, J. Layer-by-Layer PMIRRAS Characterization of DMPC Bilayers Deposited on a Au(111) Electrode Surface. *Langmuir* **2006**, *22* (25), 10365–10371.

(12) Stolberg, L.; Morin, S.; Lipkowski, J.; Irish, D. E. Adsorption of Pyridine at the Au (111) -Solution Interface. *J. ELectroanal Chem* **1991**, *307*, 241–262.

(13) Richer, J.; Lipkowski, J. Measurement of Physical Adsorption of Neutral Organic-Species at Solid Electrodes. *J. Electrochem. Soc.* **1986**, *133* (1), 121–128.

(14) Kunze, J.; Leitch, J.; Schwan, A. L.; Faragher, R. J.; Naumann, R.; Schiller, S.; Knoll, W.; Dutcher, J. R.; Lipkowski, J. New Method to Measure Packing Densities of Self-Assembled Thiolipid Monolayers. *Langmuir* **2006**, *22* (12), 5509–5519.

(15) Barenholz, Y.; Gibbes, D.; Litman, B. J.; Goll, J.; Thompson, E.; Carlson, F.D.; A Simple Method for the Preparation of Homogeneous Phospholipid Vesicles.

Bioelectrochemistry **1977**, *16* (12), 2806–2810.

(16) Kycia, A. H.; Su, Z.; Brosseau, C. L.; Lipkowski, J.; In Situ PM–IRRAS Studies of Biomimetic Membranes Supported at Gold Electrode Surfaces Your Proof . Many Thanks for Your Assistance . "Vibrational Spectroscopy at Electrified Interfaces." In *In situ PM–IRRAS studies of biomimetic membranes supported at gold electrode surfaces*; 2013; pp 345–417.

(17) Zamlynny, V.; PhD Thesis, University of Guelph (Canada), 2002.

(18) Bertie, J. E.; Ahmed, M. K.; Eysel, H. H. Infrared Intensities of Liquids. 5. Optical and Dielectric Constants, Integrated Intensities, and Dipole Moment Derivatives of H2O and D2O at 22ºC. *J. Phys. Chem.* **1989**, *93* (6), 2210–2218.

(19) Lipert, D.L. R.J.; Porter, M.D.; Specular Reflection Spectroscopy, in "Modern Techniques in Applied Molecular Spectroscopy", F.M. Mirabella Ed, Techniques in Analytical Chemistry Series, John Wiley & Sons, Inc., New York **1998**.

(20) Liu, Y.; Chu, N.; Petrache, H. I.; Tristram-nagle, S.; Kuc, N.; Nagle, J. F. E. Palik, Handbook of Optical Constants of Solids II, Academic Press, San Diego, 1998. **2005**, *88* (April), 2626–2637.

(21) Perdew, J. P.; Ernzerhof, M.; Burke, K. Rationale for Mixing Exact Exchange with Density Functional Approximations. *J. Chem. Phys.* **1996**, *105* (22), 9982–9985.

(22) Scuseria,E.; Robb, M. A.; Cheeseman, J. R.; Scalmani, G.; Barone, V.; Mennucci, B.; Petersson, G. A.; Nakatsuji, H.; Caricato, M.; Li, X.; Hratchian, H. P.; Izmaylov, A. F.; Bloino, J.; Zheng, G. ; Sonnenberg, J. L.; Hada, M. ; Ehara, M. ; Toyota, K.; Fukuda, R.; Hasegawa, J.; Ishida, M.; Nakajima, T.; Honda, Y.; Kitao, O.; Nakai, H.; Vreven, T.; Montgomery, Jr. J. A.; Peralta, J. E.; Ogliaro, F.; Bearpark, M. ; Heyd, J. J.; Brothers, E.; Kudin, K. N.; Staroverov, V. N.; Kobayashi, R.; Normand, J.; Raghavachari, K.; Rendell, A.; Burant, J. C.; Iyengar, S. S.; Tomasi, J. ; Cossi, M.; Rega, N.; Millam, J. M.; Klene, M. ; Knox, J. E.; Cross, J. B.; Bakken, V. ; Adamo, C. ; Jaramillo, J.; Gomperts, R.; Stratmann, R. E.; Yazyev, O.; Austin, A. J.; Cammi, R.; Pomelli, C.; Ochterski, J. W.; Martin, R. L.; Morokuma, K.; Zakrzewski, V. G.; Voth, G. A.; Salvador, P.; Dannenberg, J. J.; Dapprich, S. ; Daniels, A. D.; Farkas, Ö. ; Foresman, J. B.; Ortiz, J. V.; Cioslowski, J.; Fox, D. J. Gaussian 09 (Gaussian, Inc., Wallingford CT, 2009).

(23) Gains L. G. *Insoluble Monolayers at Liquid-Gas Interfaces*, *Interscience*; New York, 1966.

(24) Messina, P. V; Prieto, G.; Manuel, J.; Fernández-leyes, M. D.; Schulz, P. C.; Sarmiento, F. Colloids and Surfaces B : Biointerfaces Thermodynamic and Elastic Fluctuation Analysis of Langmuir Mixed Monolayers Composed by Dehydrocholic Acid (HDHC) and Didodecyldimethylammonium Bromide (DDAB). **2010**, *75*, 34–41.

(25) Hauser, H.; Pascher, I.; Pearson, R. H.; Sundell, S. Preferred Conformation and Molecular Packing of Phosphatidylethanolamine and Phosphatidylcholine. *Biochimica et Biophysica Acta (BBA)-Reviews on Biomembranes* **1981**, *650*, 21–51.

(26) Horswell, S. L.; Zamlynny, V.; Li, H. Q.; Merrill, A. R.; Lipkowski, J. Electrochemical and PM-IRRAS Studies of Potential Controlled Transformations of Phospholipid Layers on Au(111) Electrodes. *Faraday Discuss.* **2002**, *121* (1), 405–422.

(27) Bizzotto, D.; Zamlynny, V.; Burgess, I.; Jeffrey, C. A.; Li, H. Q.; Rubinstein, J.; Galus, Z.; Nelson, A.; Pettinger, B.; Merrill, A. R.; Lipkowski, J. Amphiphilic and Ionic Surfactants at Electrode Surfaces. In *Interfacial Electrochemistry, Theory, Experiment*

and Applications; Wieckowski, A., Ed.; 1999; p 405−426.

(28) Burgess, I.; Li, M.; Horswell, S. L.; Szymanski, G.; Lipkowski, J.; Majewski, J.; Satija, S. Electric Field-Driven Transformations of a Supported Model Biological Membrane--an Electrochemical and Neutron Reflectivity Study. *Biophys. J.* **2004**, *86* (3), 1763–1776.

(29) Lipkowski, J.; Shi, Z., Chen; A., Pettinger, B.; Bilger, C. Ionic Adsorption at the Au(111) Electrode Surface. *Electrochim. Acta* **1998**, *43* (19–20), 2875–2888.

(30) Madrid, E.; Horswell, S. L. Effect of Electric Field on Structure and Dynamics of Bilayers Formed from Anionic Phospholipids. *Electrochim. Acta* **2014**, *146*, 850–860.

(31) Dluhy, R. A.; Mendelsohn, R.; Casal, H. L.; Mantsch, H. H. Interaction of Dipalmitoylphosphatidylcholine and Dimyristoylphosphatidylcholine-D54 Mixtures with Glycophorin. A Fourier Transform Infrared Investigation. *Biochemistry* **1983**, *22* (5), 1170–1177.

(32) Casal, H. L.; Mantsch, H. H. Polymorphic Phase Behaviour of Phospholipid Membranes Studied by Infrared Spectroscopy. *Biochim. Biophys. Acta* **1984**, *779* (4), 381–401.

(33) Mantsch, H. H.; McElhaney, R. N. Phospholipid Phase Transitions in Model and Biological Membranes as Studied by Infrared Spectroscopy. *Chem. Phys. Lipids* **1991**, *57* (2–3), 213–226.

(34) Banyay, M; Sarka, M; Graslund, A. A Library of IR Bands of Nucleic Acids in Solution. *Biophys. Chem.* **2003**, *104*, 477–488.

(35) Nishimura, Y.; Tsuboi, M. In-Plane Vibrational Modes of Cytosine from an Ab Initio MO Calculation. *Chem. Phys.* **1985**, *98* (1), 71–80.

(36) Kulihska, K.; Sarzyiiska, J.; Wiewiorowski, M. Differences in the Association Abilities in Aqueous Solutions of Cytidine , 2 ’-Deoxycytidine and Their Phosphate Salts Studied by Fourier Transform Infrared Spectroscopy. *Vib. Spectrosc.* **1991**, *1*, 277–286.

(37) Surewicz, W.; Mantsch, H. New Insight into Protein Secondary Structure from Resolution-Enhanced Infrared Spectra. *Biochim. Biophys. Acta* **1988**, *952* (2), 115–130.

(38) Mathlouthi, M; Seuvre, A. M. F.T.I.R and Laser-Raman Spectra of Cytosine and Cytidine. *Carbohydr. Res.* **1986**, *146*, 1–13.

(39) Tsuboi, M. Application of Infrared Spectroscopy to Structure Studies of Nucleic Acids. *Appl. Spectrosc. Rev.* **1970**, *3*, 45–90.

(40) Susi, H.; Ard, J. S.; Purcell, J. M. Vibrational Spectra of Nucleic Acid Constituents-II. Planar Vibrations of Cytosine. *Spectrochim. Acta* **1973**, *29* (4), 725–733.

(41) Seuvre, A.-M.; Mathlouthi, M. F.T.-I.R. Spectra of Oligo- and Poly-Nucleotides. *Carbohydr. Res.* **1987**, *169* (C), 83–103.

(42) Alvarez-Malmagro, J.; PhD Thesis, University of Seville (Spain), 2017.

(43) Lewis, R. N.; McElhaney, R. N.; Pohle, W.; Mantsch, H. H. Components of the Carbonyl Stretching Band in the Infrared Spectra of Hydrated 1,2-Diacylglycerolipid Bilayers: A Reevaluation. *Biophys. J.* **1994**, *67* (6), 2367–2375.

(44) Nowak, M. J.; Lapinski, L.; Fulara, J. Matrix Isolation Studies of Cytosine: The Separation of the Infrared Spectra of Cytosine Tautomers. *Spectrochim. Acta Part A*

Mol. Spectrosc. **1989**, *45* (2), 229–242.

(45) Lee, C.; Park, K. H.; Cho, M. Vibrational Dynamics of DNA. I. Vibrational Basis Modes and Couplings. *J. Chem. Phys.* **2006**, *125* (11).

(46) Starikov, E.B.; Semenov, M. IR-Spectroscopic and Quantum-Chemical Study of Hydration of Citidine-5'- Monophsphate Disodium Salts. *Zh.Fiz.Khim* **1988**, *62*, 2120–2126.

(47) Borah, B; Wood, J.; The Cytidinium-Cytidine Complex: Infrared and Raman Spectroscopic Studies. *J. Mol. Struct.* **1976**, *30*, 13–30.